Excitonic Creation of Highly Luminescent Defects In Situ in Working Organic Light-Emitting Diodes

Yong-Biao Zhao, Grayson L. Ingram, Xi-Wen Gong, Xi-Yan Li, Li-Na Quan, Pei-Cheng Li, Jia-Qi Xie, Edward H. Sargent, and Zheng-Hong Lu**

Excitons play the central role in organic optoelectronic devices. Efficient exciton-to-photon and photon-to-electron conversion promote quantum yield in optoelectronic devices such as organic light-emitting diodes and organic solar cells. Exciton-related reaction products and defects in working devices have previously been viewed as fatal to stability. Here, the utilization of these excitonic reactions to create luminescent defects with extremely high (6.7%) external quantum efficiency in an operating device containing 1,1-bis((di-4-tolylamino)-phenyl) cyclohexane (TAPC) is reported. Transient photoluminescence reveals a long delayed fluorescence lifetime (2.7 µs) from these emissive defects, indicating that they exhibit thermally activated delayed fluorescence. It is shown that the functional group of tri-*p*-tolylamine (TPTA) follows similar processes as TAPC, suggesting that the chemical nature of the observed luminescent defects is directly related to TPTA.

1. Introduction

Excitonic processes dictate the operation of organic optoelectronic devices.[1–13] In-depth understanding and innovative engineering of excitons in devices are central topics for the organic semiconductor community. For example, in organic light-emitting diodes (OLEDs),[14] exciton dynamics, such as formation, recombination, energy transfer, and annihilation, govern overall device performance. Excitonic processes are also useful for in situ synthesis of organic semiconductors by activating bond dissociation and formation, found to be more efficient than traditional wet chemical synthesis methods.[15,16] However, some excitonic processes in optoelectronic devices can cause fatal stability issues, triggering the formation of defective species in working devices and resulting in device degradation.[17–20] Degradation was found to be more rapid for most wide bandgap materials[20] due to the fact that the exciton energy in these materials is comparable with or even higher than the dissociation energy of key chemical bonds.

Among these large-bandgap organic semiconductors, 1,1-bis((di-4-tolylamino) phenyl) cyclohexane (TAPC) has been widely studied.[14,21] TAPC is a popular hole transporting material (HTM) for OLEDs owing to its high hole mobility (10^{-2} cm^2 V^{-1} s^{-1}).[22] More importantly, its high triplet energy (2.98 eV)[23] is helpful for the confinement of triplet excitons to the emissive layer (EML) in high efficiency OLEDs, especially blue phosphorescent OLEDs.[24,25] However, the instability of TAPC associated with its large bandgap is of concern for practical applications.[26] Adachi et al. studied a series of HTMs and found that TAPC-based devices showed the lowest stability.[26] Kwon et al. also found that OLEDs with TAPC hole transporting layer (HTL) next to the EML usually exhibit much shorter operational lifetimes; and that the addition of another HTL between TAPC and the EML can greatly improve device stability.[27] The degradation of TAPC is usually accompanied by the formation of low energy defect emission at around 590 nm. The first observation of defect emission from TAPC was reported by Kalinowski et al. in a device with a structure indium tin oxide (ITO)/TAPC/Ca.[28] More recently, researchers have carried out studies on the chemical transformation processes of TAPC under electrical stressing.[18,29] For example, Kondakov examined degradation of OLEDs using TAPC HTL.[18] He performed density functional calculations which predicted that the dissociation energies of some bonds in TAPC were quite low (around 75 kcal mol^{-1}) and experimentally identified the presence of several degradation products formed through cleavage of these bonds in degraded OLEDs. Recently, Wang et al. examined the stabilities of a few HTMs that were commonly used in phosphorescent OLEDs.[20] They identified the exciton-driven degradation mechanism and found that the larger the bandgap, the faster the rate of chemical transformation. These previous works suggest that the high excited state energies played a significant role in the chemical transformation processes. However, as the chemical degradation processes usually happen at the interface between HTL and EML, it is quite difficult to carry

Dr. Y.-B. Zhao, G. L. Ingram, P.-C. Li, J.-Q. Xie, Prof. Z.-H. Lu
Department of Materials Science and Engineering
University of Toronto
184 College Street, Toronto, Ontario M5S 3E4, Canada
E-mail: zhenghong.lu@utoronto.ca

Dr. Y.-B. Zhao, X.-W. Gong, Dr. X.-Y. Li, Dr. L.-N. Quan, Prof. E. H. Sargent
Department of Electrical and Computer Engineering
University of Toronto
35 St George Street, Toronto, Ontario M5S 1A4, Canada
E-mail: ted.sargent@utoronto.ca

Prof. Z.-H. Lu
Department of Physics
Yunnan University
Kunming, Yunnan 650091, China

The ORCID identification number(s) for the author(s) of this article can be found under https://doi.org/10.1002/adom.201700856.

DOI: 10.1002/adom.201700856

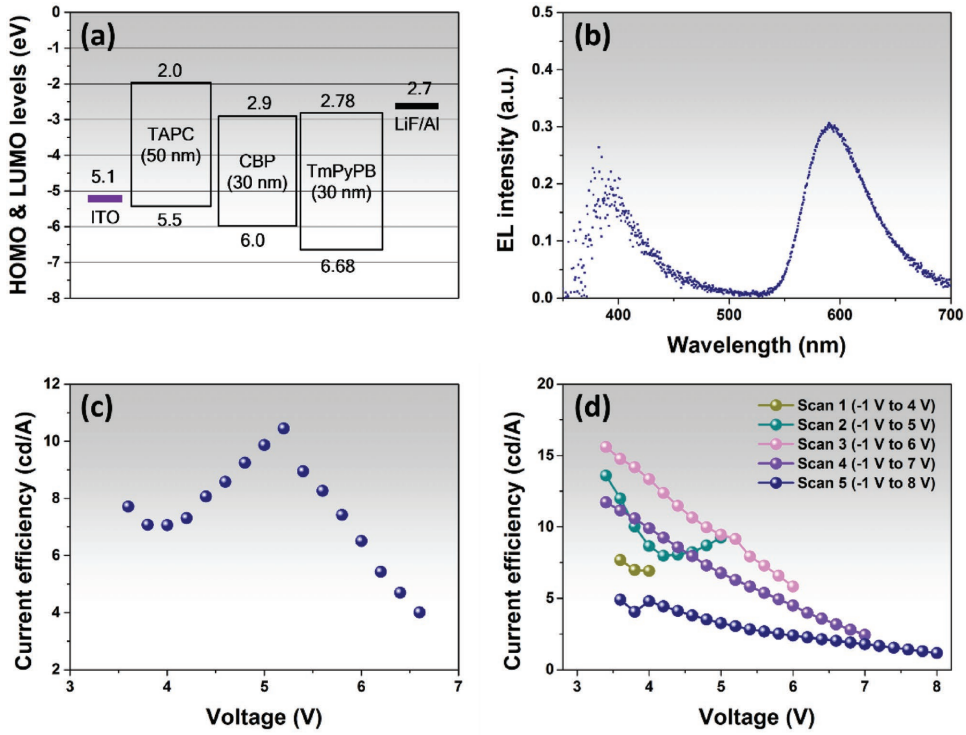

Figure 1. a) Optimized device structure and energy level diagram. b) Typical EL spectrum of the device at 7 V. c) *J–V* characteristic of the optimized device. d) *J–V* characteristic of the optimized device during repeated *J–V* scan cycles.

out detailed photophysical and chemical studies on the defects because of the too low quantity.[18,27]

In this work, we present new findings on luminescent TAPC degradation products. First, these luminescent defects can produce a surprisingly efficient emission, greater than the theoretical limit for normal fluorescent emitters. Second, straightforward photophysic evidence supports the irreversible chemical transformation of TAPC. Third, transient photoluminescence (PL) of the defects reveals an ultralong 2.7 µs excited state lifetime, indicating emission from thermally activated delayed fluorescence (TADF).[30–33] Finally, tri-*p*-tolylamine (TPTA), the core building block of TAPC, is found to be responsible for the formation of the luminescent defects.

2. Results and Discussions

2.1. Formation of High External Quantum Efficiency (EQE) Luminescent Defects

The device structure used in our study is ITO/TAPC (50 nm)/4,4-N,N′-Dicarbazole-1,1′-biphenyl (CBP) (30 nm)/1,3,5-Tri[(3-pyridyl)-phen-3-yl]benzene (TmPyPB) (30 nm)/LiF (1 nm)/Al (100 nm) (see **Figure 1**a). As shown in Figure S1 (Supporting Information), the device turns on (when luminance reaches 1 cd m^{-2}) at around 3.6 V and a maximum luminance of 890 cd m^{-2} is achieved at 6.4 V. The device shows an orange emission band peaking at 590 nm (as shown in Figure 1b), similar to the one observed from a previous publication.[28] The current efficiency versus voltage (CE–*V*) curve is shown in Figure 1c. As shown in the figure, the CE–*V* plot

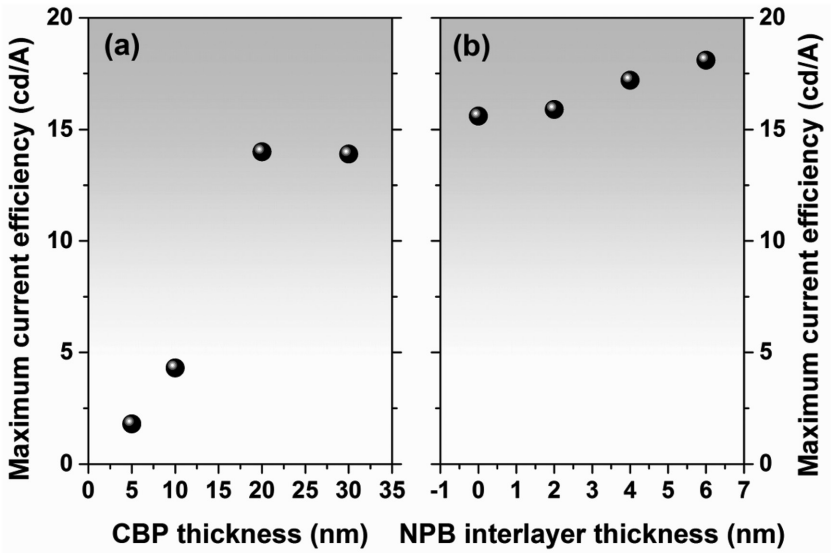

Figure 2. a) The effect of CBP thickness on maximum current efficiency in device ITO/TAPC (50 nm)/CBP (x = 5, 10, 20, and 30 nm)/TmPyPB (30 nm)/LiF (1 nm)/Al (100 nm). b) The effect of NPB interlayer thickness on maximum current efficiency in device ITO/TAPC (50 nm)/CBP (30 nm)/ NPB (x = 0, 2, 4, and 6 nm)/TmPyPB (30 nm)/LiF (1 nm)/Al (100 nm).

is quite different from that of common OLEDs, where the CE either rolls off gradually or increases to a maximum and then decreases.[34,35] The CE–*V* of our device shows a dip followed by a rapid increase in CE and subsequent roll-off. The peak CE is 10.5 cd A^{-1}, which corresponds to an EQE of 3.9%. This abnormal behavior of CE deserves further investigation. Wang et al. have studied the growth dynamics of the TAPC 590 nm emission band in a device with the structure ITO/MoO_3 (5 nm)/TAPC (30 nm)/1,3,5-Tris(1-phenyl-1Hbenzimidazol-2-yl)benzene (TPBi) (30 nm)/LiF (0.5 nm)/Al.[20] These authors found that, when their device was driven continuously at 20 mA cm^{-2}, the 590 nm emission increases first and then decreases after reaching a maximum. Intrigued by this phenomenon, we explored the growth dynamics by electrically stressing one device from –1 to 4, 5, 6, 7, and 8 V, repeatedly. As shown in Figure S2 (Supporting Information), the current density shows a slight increase after each current density–voltage (*J*–*V*) sweep, while the turn-on voltage decreases from 3.6 to 3.3 V after the third *J*–*V* sweep. At the same time, there is about 2.8 times improvement in luminance compared to 1.5 times increase in *J*. This corresponds to twofold increase in CE at the third *J*–*V* sweep relative to the first *J*–*V* sweep, as shown in Figure 1d. Additional *J*–*V* sweeps do not improve the CE further. At the fifth *J*–*V* sweep, there is an obvious increase in turn-on voltage and decrease in luminance, indicating the formation of quenching defects. From Figure 1c, it is also clear that the fast CE roll-off occurs at a threshold voltage of 5.3 V, which agrees with the CE drop after the third *J*–*V* sweep. These results indicate that the efficiency of these defect species grow gradually upon electrical stress. Remarkably, a maximum CE of 15.6 cd A^{-1} is achieved during the third sweep, corresponding to an EQE of 5.8%.

This CE greatly exceeds any documented value based on TAPC degradation defects.[20,28] By comparing the device structure used here with those in previous reports, we note that the TAPC was adjacent to the electron transporting layer (ETL) in the previous literature, whereas in our case, a bipolar CBP layer is placed between the TAPC and the ETL. This indicates that the direct interaction with electrons and holes on TAPC may produce additional quenching sources. To prove this, we examined the effect of CBP thickness on device performance using thicknesses of 5, 10, 20, and 30 nm. As shown in Figure S3b (Supporting Information), the current density decreases as the thickness of CBP increases, as expected. As shown in Figure S3c (Supporting Information), the turn-on voltage decreases from 4 to around 3.4 V, accompanied by an increase in CE (Figure S3d, Supporting Information). The maximum CEs for each CBP thicknesses are plotted in **Figure 2**a. As shown in Figure 2a, when the thickness of CBP increases from 5 to 20 nm, the maximum efficiency of the device increases more than 6 times from below 2 to above 13 cd A^{-1}. This indicates that distancing electrons and recombination zone from the TAPC layer is key to make efficient light-emitting TAPC defects. Based on this finding, we expect further improvement in the device performance by introducing a layer of *N,N* -bis(naphthalen-1-yl)-*N,Ns*-bis(phenyl)benzidine (NPB), which will create a higher electron injection barrier (see Figure S4 in the Supporting Information for energy level diagram), between CBP and TmPyPB. We experimented the devices with NPB interlayer of different thicknesses by the repeated *J*–*V* scan method (see Figure S4 in the Supporting Information for detailed CE–*V* plots) and we optimized the processes to obtain a CE higher than 18 cd A^{-1} (corresponding to an EQE of 6.7%) as shown in Figure 2b. This is above the theoretical limit for a fluorescent material.

2.2. Time Dependence

To gain a deep understanding of the electroluminescence (EL) process, we performed a time-resolved EL study.[20] Figure S5 (Supporting Information) shows the EL dynamics of the device ITO/TAPC (50 nm)/CBP (30 nm)/TmPyPB (30 nm)/LiF (1 nm)/Al (100 nm) as a function of the stressing time. All the EL spectra contain two emission bands: a blue band due to the emission from CBP and/or TAPC and an orange band due to the emission of TAPC degradation defects. The intensities of the blue and orange bands are integrated and shown in **Figure 3**a,b. It is observed that the blue band decreases gradually, while the orange band increases and then decreases after reaching a maximum. The cocurrent increase of orange band and decrease of

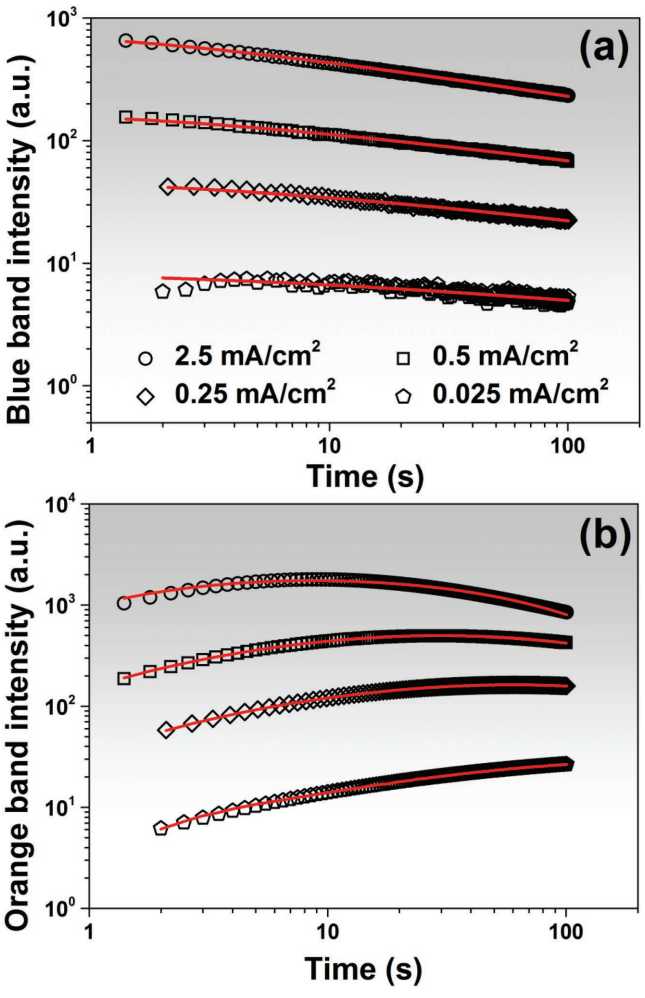

Figure 3. Calculated a) blue and b) orange emission intensity as a function of time for the time-resolved EL spectra in Figure S5 (Supporting Information) and the corresponding fitting curves (red lines) for both the blue and orange emission bands.

blue band indicates energy transfer from the host to the degradation defects. This energy transfer process can be quantified using an excitonic energy transfer model (see the Supporting Information). The time required for the orange emission to reach its maximum, i.e., defect formation rate, decreases as the stressing current density increases. Higher current density generates higher exciton concentration. This is consistent with exciton driven degradation processes.[17]

2.3. Steady-State and Transient Photoluminescence (PL) Study

We have also measured the steady-state PL of the device before and after the electrical stressing. For PL experiment, we fabricated large area (around 1 × 1 cm^2) devices with the structure ITO/TAPC (50 nm)/CBP (30 nm)/TmPyPB (30 nm)/LiF (1 nm)/Al (100 nm). The PL spectra of the device before and after a −1 to 6 V *J*–*V* scan were shown in Figure S6 (Supporting Information). The PL spectra show a strong emission in the blue region, which originates from emission of TAPC, CBP, and TmPyPB. After electrical stressing, a small peak emerges in the orange region. The orange region is shown in **Figure 4**a. The device before the electrical stressing does not show any spectral feature from 550 to 650 nm (only a tail extended from the blue emission). After being electrically stressed, the device shows an additional orange emission band peaked at 589 nm. This PL band is identical to the EL band of TAPC degradation defects. This indicates that the luminescent defects are not a transient electrical phenomenon; the luminescent defects are new and stable species.

As shown above, the best device has a maximum EQE of 6.7%, indicating that the emission may be due to TADF. To examine whether the orange emission from the TAPC degradation defects is due to TADF, we carried out a transient PL decay study on the TAPC device that had undergone a −1 to 6 V *J*–*V* scan. Figure 4b shows the PL decay at 590 nm, which indeed shows fast and slow decay components. The fast component can be fitted with two exciton lifetimes of 3.5 and 29.1 ns, while the slow component can be fitted with a very long exciton lifetime of 2752 ns. The 3.5 ns exciton lifetime is due to the decay of the tail emission of the 400 nm peak (see Figure 4a), which can be verified by a similar 3.1 ns exciton lifetime that is probed at 400 nm (see Figure 4b inset). The other two exciton lifetimes of 29.1 and 2752 ns are due to the decay of TAPC degradation defects. The coexistence of fast (ns) and slow (μs) exciton lifetimes is a characteristic of TADF emitters.[30–33] The fast decay component originates from singlet emission, while the slow decay component is from the delayed emission due to reverse intersystem crossing from triplet to singlet states. Based on the high EQE and long delayed exciton lifetime from TAPC degradation defects, we conclude that TAPC degrades into efficient TADF-type species.

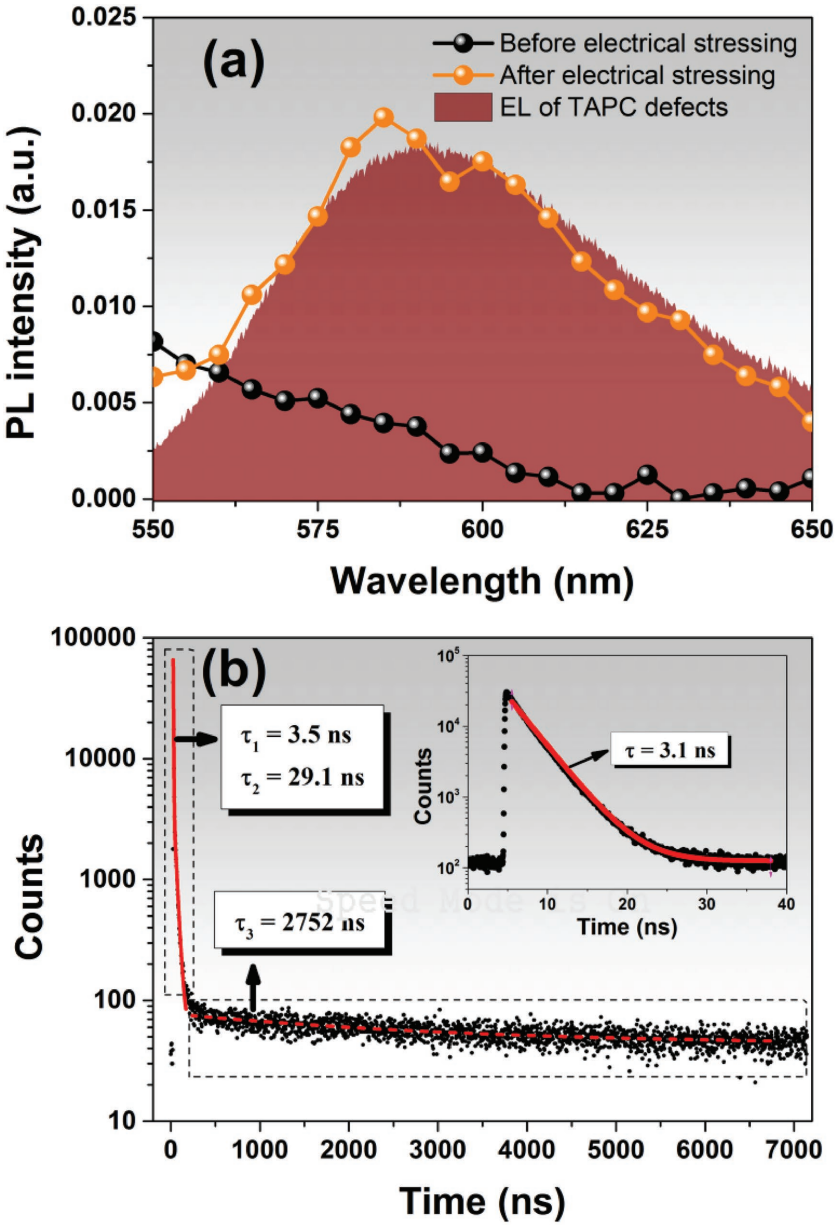

Figure 4. a) Steady-state PL from device ITO/TAPC (50 nm)/CBP (30 nm)/TmPyPB (30 nm)/LiF (1 nm)/Al (100 nm) before and after electrical stressing, and EL of the device with same structure. b) Transient PL probed at 590 nm of device ITO/TAPC (50 nm)/CBP (30 nm)/TmPyPB (30 nm)/LiF (1 nm)/Al (100 nm) after electrical stressing. Inset of (b): Transient PL probed at 400 nm of the same device.

2.4. Source for Producing Luminescent Defect

The 590 nm emission bands have been observed in several materials, such as TAPC, 5′-[4-[bis(4-ethylphenyl)amino]-

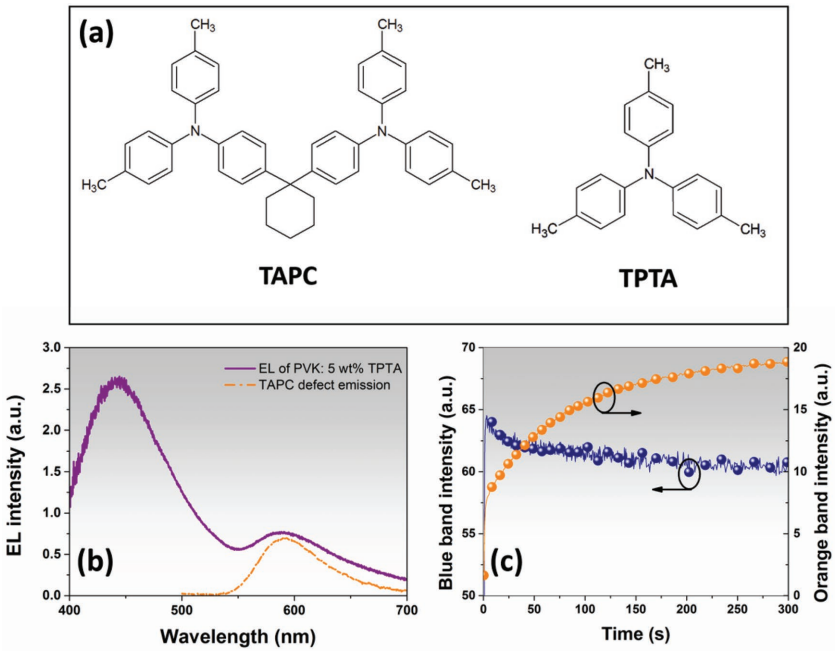

Figure 5. a) Molecular structures of TAPC and TPTA. b) EL spectrum of device ITO/PEDOT:PSS/PVK: 5 wt% TPTA (40 nm)/TPBi (65 nm)/LiF (1 nm)/Al (100 nm) and EL spectrum of TAPC degradation byproduct. c) Calculated blue and orange band intensity from time resolved EL spectra (Figure S7, Supporting Information) of ITO/PEDOT:PSS/PVK: 5 wt% TPTA (40 nm)/TPBi (60 nm)/LiF (1 nm)/Al (100 nm).

phenyl]-*N*,*N*,*N*′,*N*′-tetrakis(4-ethylphenyl)-[1,1′:3′,1″-terphenyl]-4,4″-diamine,[36] 9,9-bis [4-(di-*p*-tolyl)aminophenyl]-2,7-bis(diphenylamino)fluorene,[37] and 9,9-bis[4-(di-*p*-tolyl)-aminophenyl]-2,7-bis(9-carbazolyl)fluorine.[37] All of these materials have the same building block: TPTA, as shown in **Figure 5**a, and thus we suspect that TPTA may be responsible for the degradation process. It is worth investigating whether or not TPTA itself also shows similar EL properties. We fabricated a TPTA-based OLED with device structure of ITO/Poly(3,4-ethylenedioxythiophene)-poly(styrenesulfonate) (PEDOT:PSS) (40 nm)/poly(9-vinylcarbazole) (PVK): 5 wt% TPTA (40 nm)/TPBi (60 nm)/LiF (1 nm)/Al (100 nm), where PVK serves as the host for TPTA. The *J*–*V* and *L*–*V* curves for the device are shown in Figure S7a (Supporting Information). As shown in the figure, the device has a turn-on voltage of 4.8 V and maximum luminance of 70 cd m^{-2}. Interestingly, the CE–*V* plot shows a similar trend as in Figure 1b, which indicates that similar degradation processes happen within the TPTA- and TAPC-based devices. A typical EL spectrum for the device is shown in Figure 5b. The EL spectrum shows two main emission bands. The band peaked around 450 nm is due to the emission from TPTA excimers, as observed by Kalinowski et al.,[28] while the other band is peaked at the same wavelength as the TAPC degradation defects. We studied the time-resolved EL spectra for the TPTA device at a constant current density of 0.25 mA cm^{-2}, which is shown in Figure S7c (Supporting Information). The intensities for the blue and orange bands are extracted and plotted in Figure 5c, which again resemble the time dependent EL of TAPC in Figure 4. Based on these findings, we conclude that TPTA is the functional group that undergoes transformation, resulting in the observed 590 nm emission.

Attempts to measure energy levels of the degradation products have been made. However, the signal-to-noise ratio in the ultraviolet photoelectron spectroscopy measurement is too low to reveal any meaningful information. Similarly, other experimental attempts to determine the chemical structure of the degradation products have been proven difficult.

3. Conclusion

In conclusion, we report that an in situ excitonic reaction method can be used to produce highly luminescent (with an EQE as high as 6.7%) species in a working OLED containing TAPC. We demonstrate that this emission is of TADF characteristics as evidenced by the observation of long exciton lifetime of microsecond scale. We found that TPTA is responsible for the observed orange emission from various TPTA-containing organic materials including TAPC. This work demonstrates that electrical stressing can lead to formation of highly efficient luminescent materials in working devices. It indicates the possibility of in situ in device fabricating of luminescent compounds by electrical method. In our work, we have shown that derivatives of TPTA could be electrically stresses to yield high performance TADF emitters. The formation of electrically generated luminescent defects shall also provide a very useful tool to understand the electrical degradation of organic molecules in OLEDs.

4. Experimental Section

Device Fabrication and Characterization: All OLEDs were fabricated by thermal evaporation using a customized tool under a base pressure of 10^{-8} Torr on a glass substrate (1.1 mm thick) precoated with ITO, having a thickness and sheet resistance of 120 nm and 15 Ω sq^{-1}, respectively. Prior to loading, the substrate was degreased with standard solvents, blow-dried using a N_2 gun, and treated in a UV-ozone chamber. The active area for each device was 2 mm^2. For the PL study, a 1 cm^2 active area was used. The deposited layer thickness was monitored by a quartz crystal microbalance that was calibrated by spectroscopic ellipsometry (Sopra GES 5E). Luminance–voltage measurements were carried out using a Minolta LS-110 Luminance Meter. Current–voltage characteristics were measured using an HP4140B pA meter. The radiant flux for calculating EQEs was measured using an integrating sphere equipped with an Ocean Optics USB 4000 spectrometer with National Institute of Standards and Technology (NIST) traceable calibration using a halogen lamp.

Photoluminescence Study: Steady state photoluminescence and transient photoluminescence measurements were performed using a Horiba Fluorolog system. A pulsed UV laser diode (λ = 375 nm) was used as the excitation source and the light signal was acquired with a time correlated single photon counting detector. The instrument response function provided an overall time resolution of $\Delta t \approx 0.13$ ns.

Supporting Information

Supporting Information is available from the Wiley Online Library or from the author.

Acknowledgements

This work was funded by the Natural Sciences and Engineering Research Council of Canada, the National Natural Science Foundation of China (Grant No. U1402273), and the Connaught Global Challenge Fund of the University of Toronto. The research infrastructure funding was provided by the Canada Foundation for Innovation and the Ontario Research Fund – Research Infrastructure.

Conflict of Interest

The authors declare no conflict of interest.

Keywords

degradation, excitons, luminescent defects, organic light-emitting diodes, thermally activated delayed fluorescence

Received: August 14, 2017
Revised: October 17, 2017
Published online: December 21, 2017

[1] F. Deschler, E. Da Como, T. Limmer, R. Tautz, T. Godde, M. Bayer, E. von Hauff, S. Yilmaz, S. Allard, U. Scherf, J. Feldmann, *Phys. Rev. Lett.* **2011**, *107*, 127402.
[2] J. M. Hodgkiss, S. Albert-Seifried, A. Rao, A. J. Barker, A. R. Campbell, R. A. Marsh, R. H. Friend, *Adv. Funct. Mater.* **2012**, *22*, 1567.
[3] Q. S. Zhang, T. Komino, S. P. Huang, S. Matsunami, K. Goushi, C. Adachi, *Adv. Funct. Mater.* **2012**, *22*, 2327.
[4] G. Grancini, M. Maiuri, D. Fazzi, A. Petrozza, H. J. Egelhaaf, D. Brida, G. Cerullo, G. Lanzani, *Nat. Mater.* **2013**, *12*, 29.
[5] E. Jailaubekov, A. P. Willard, J. R. Tritsch, W. L. Chan, N. Sai, R. Gearba, L. G. Kaake, K. J. Williams, K. Leung, P. J. Rossky, X. Y. Zhu, *Nat. Mater.* **2013**, *12*, 66.
[6] S. Kena-Cohen, S. A. Maier, D. D. C. Bradley, *Adv. Opt. Mater.* **2013**, *1*, 827.
[7] K. Kolata, T. Breuer, G. Witte, S. Chatterjee, *ACS Nano* **2014**, *8*, 7377.
[8] W. J. Li, Y. Y. Pan, R. Xiao, Q. M. Peng, S. T. Zhang, D. G. Ma, F. Li, F. Z. Shen, Y. H. Wang, B. Yang, Y. G. Ma, *Adv. Funct. Mater.* **2014**, *24*, 1609.
[9] V. Mikhnenko, M. Kuik, J. Lin, N. van der Kaap, T. Q. Nguyen, P. W. M. Blom, *Adv. Mater.* **2014**, *26*, 1912.
[10] M. Tabachnyk, B. Ehrler, S. Gelinas, M. L. Bohm, B. J. Walker, K. P. Musselman, N. C. Greenham, R. H. Friend, A. Rao, *Nat. Mater.* **2014**, *13*, 1033.
[11] S. R. Forrest, *Philos. Trans. R. Soc. A* **2015**, *373*, 20140320.
[12] V. Mikhnenko, P. W. M. Blom, T. Q. Nguyen, *Energy Environ. Sci.* **2015**, *8*, 1867.
[13] S. M. Menke, R. J. Holmes, *J. Phys. Chem. C* **2016**, *120*, 8502.
[14] C. W. Tang, S. A. VanSlyke, *Appl. Phys. Lett.* **1987**, *51*, 913.
[15] Y.-L. Chang, Y.-L. Rao, S. Gong, G. L. Ingram, S. Wang, Z.-H. Lu, *Adv. Mater.* **2014**, *26*, 6729.
[16] S. Wang, D.-T. Yang, J. Lu, H. Shimogawa, S. Gong, X. Wang, S. K. Mellerup, A. Wakamiya, Y.-L. Chang, C. Yang, Z.-H. Lu, *Angew. Chem., Int. Ed.* **2015**, *54*, 15074.
[17] N. C. Giebink, B. W. D'Andrade, M. S. Weaver, P. B. Mackenzie, J. J. Brown, M. E. Thompson, S. R. Forrest, *J. Appl. Phys.* **2008**, *103*, 044509.
[18] D. Y. Kondakov, *J. Appl. Phys.* **2008**, *104*, 084520.
[19] F. So, D. Kondakov, *Adv. Mater.* **2010**, *22*, 3762.
[20] Q. Wang, B. Sun, H. Aziz, *Adv. Funct. Mater.* **2014**, *24*, 2975.
[21] C. W. Tang, S. A. VanSlyke, C. H. Chen, *J. Appl. Phys.* **1989**, *65*, 3610.
[22] P. M. Borsenberger, L. Pautmeier, R. Richert, H. Bässler, *J. Chem. Phys.* **1991**, *94*, 8276.
[23] K. Goushi, R. Kwong, J. J. Brown, H. Sasabe, C. Adachi, *J. Appl. Phys.* **2004**, *95*, 7798.
[24] N. Chopra, J. Lee, Y. Zheng, S.-H. Eom, J. Xue, F. So, *Appl. Phys. Lett.* **2008**, *93*, 143307.
[25] N. Chopra, J. S. Swensen, E. Polikarpov, L. Cosimbescu, F. So, A. B. Padmaperuma, *Appl. Phys. Lett.* **2010**, *97*, 033304.
[26] C. Adachi, K. Nagai, N. Tamoto, *Appl. Phys. Lett.* **1995**, *66*, 2679.
[27] S. Kwon, K.-R. Wee, C. Pac, S. O. Kang, *Org. Electron.* **2012**, *13*, 645.
[28] J. Kalinowski, G. Giro, M. Cocchi, V. Fattori, P. Di Marco, *Appl. Phys. Lett.* **2000**, *76*, 2352.
[29] S. Scholz, D. Kondakov, B. Lüssem, K. Leo, *Chem. Rev.* **2015**, *115*, 8449.
[30] H. Uoyama, K. Goushi, K. Shizu, H. Nomura, C. Adachi, *Nature* **2012**, *492*, 234.
[31] K. Shizu, M. Uejima, H. Nomura, T. Sato, K. Tanaka, H. Kaji, C. Adachi, *Phys. Rev. Applied* **2015**, *3*, 014001.
[32] S. Hirata, Y. Sakai, K. Masui, H. Tanaka, S. Y. Lee, H. Nomura, N. Nakamura, M. Yasumatsu, H. Nakanotani, Q. Zhang, K. Shizu, H. Miyazaki, C. Adachi, *Nat. Mater.* **2015**, *14*, 330.
[33] S. Y. Lee, T. Yasuda, H. Komiyama, J. Lee, C. Adachi, *Adv. Mater.* **2016**, *28*, 4019.
[34] N. C. Giebink, S. R. Forrest, *Phys. Rev. B* **2008**, *77*, 235215.
[35] C. Murawski, K. Leo, M. C. Gather, *Adv. Mater.* **2013**, *25*, 6801.
[36] J. Rommens, A. Vaes, M. van der Auweraer, F. C. D. Schryver, H. Bässler, H. Vestweber, J. Pommerehne, *J. Appl. Phys.* **1998**, *84*, 4487.
[37] X. Xu, G. Yu, C. Di, Y. Liu, K. Shao, L. Yang, P. Lu, *Appl. Phys. Lett.* **2006**, *89*, 123503.